Наносистеми, наноматеріали, нанотехнології
Nanosistemi, Nanomateriali, Nanotehnologii
2021, т. 19, № 4, сс. 981–996

PACS numbers: 61.05.cp, 61.72.Hh, 68.37.Hk, 78.40.Fy, 78.67.Bf, 87.19.xb, 87.19.xg

Structural, Morphological and Optical Properties of Manganese (Mn) and Gadolinium (Gd) Ions-Doped ZnO Nanoparticles and Their Antimicrobial Activity

Abebe Belay Gemta and Diriba Tsegaye

Department of Applied Physics,
Adama Science and Technology University,
P.O. Box, 1888 Adama, Ethiopia

In this research, ZnO nanoparticles are doped with the manganese (Mn) and gadolinium (Gd) ions using chemical co-precipitation method. The effects of dopants on the structural, morphological and optical properties of ZnO are investigated. In addition, the antimicrobial activity of ZnO nanoparticles doped with the Mn and Gd metallic ions are revealed. The structural, morphological and optical properties are characterized using x-ray diffraction (XRD), scanning electron microscopy (SEM) and ultraviolet-visible (UV-Vis) spectroscopy. The XRD results reveal the synthesized nanoparticles possessed hexagonal phase of wurtzite structure and average crystallite size of 31–38 nm. The decreases in crystallite size, lattice parameters, unit volume and bond length are observed after incorporation of the Mn and Gd ions into the ZnO matrix. On the other hand, increments in strain and concentration of defects are observed after the Mn and Gd doping. Scanning electron-microscopy images show spherical shape with well-defined distributions observed. The energy band gaps estimated from ultraviolet-visible absorption spectra are found to be 3.35, 3.28 and 3.07 eV for undoped ZnO, Gd-doped and Mn-doped ones, respectively. The antimicrobial activity of undoped, Mn- and Gd-doped ZnO nanoparticles are tested against gram-negative bacteria (*E. coli* and *P. aeruginosa*), gram-positive bacteria (*S. aureus* and *B. subtilis*) and fungus (*C. albicans*) using agar-well diffusion method. The results indicate that the antimicrobial activity of doped ZnO nanoparticles is higher as compared to undoped ZnO nanoparticles. As also found, the gram-positive bacteria are more susceptible to ZnO nanoparticle than gram-negative bacteria and fungus.

У цьому дослідженні наночастинки ZnO леґуються йонами Манґану (Mn) та Ґадолінію (Gd) за допомогою хемічного методу співосадження. Досліджено вплив леґування на структурні, морфологічні й оптичні властивості ZnO. Крім того, виявлено антимікробну активність наночастинок ZnO, леґованих металічними йонами Mn і Gd. Структурні, мор-

фологічні й оптичні властивості характеризуються за допомогою рентґенівської дифракції (РД), сканувальної електронної мікроскопії і спектроскопії у видимій та ультрафіолетовій областях світла. Результати РД показують, що синтезовані наночастинки мали гексагональну фазу структури вюрциту та середній розмір кристаліту у 31–38 нм. Зменшення розміру кристаліту, параметрів ґратниці, об'єму елементарної комірки та довжини зв'язку спостерігаються після втілення йонів Mn та Gd до матриці ZnO. З іншого боку, збільшення деформації та концентрації дефектів спостерігаються після леґування Mn і Gd. Сканувальні електронно-мікроскопічні зображення показують сферичну форму з чітко визначеними розподілами, що спостерігаються. Енергетичні зонні щілини, оцінені з ультрафіолетово-видимих спектрів поглинання, виявилися у 3,35, 3,28 і 3,07 еВ для нелеґованого ZnO та леґованого Gd і Mn відповідно. Антимікробна активність нелеґованих та леґованих Mn і Gd наночастинок ZnO перевіряється проти грамнеґативних бактерій (*E. coli* і *P. aeruginosa*), грампозитивних бактерій (*S. aureus* і *B. subtilis*) і грибка (*C. albicans*) за допомогою імунодифузійного методу в агаровому ґелі. Результати показують, що антимікробна активність леґованих наночастинок ZnO вище в порівнянні з нелеґованими наночастинками ZnO. Як також з'ясувалося, грампозитивні бактерії більш сприйнятливі до наночастинок ZnO, ніж грамнеґативні бактерії та грибок.

Key words: $Zn_{0.98}Mn_{0.02}O$, $Zn_{0.98}Gd_{0.02}O$, co-precipitation method, structure, antimicrobial activity.

Ключові слова: $Zn_{0.98}Mn_{0.02}O$, $Zn_{0.98}Gd_{0.02}O$, метод співосадження, структура, протимікробна активність.

(Received 11 December, 2020; in revised form, 31 December, 2021)

1. INTRODUCTION

Nanoparticles (NPs) are special classes of organic or inorganic materials having size in the range of 1 to 100 nm in at least one dimension. They have unique and enhanced functional properties such as high surface area to volume ratio and more atoms on their surface than their micro- or macro-scale counterparts owing to their nanoscale feature [1]. Metal oxide nanoparticles are important materials, finding applications in a diverse range of activities. Among them, ZnO NPs have many significant features such as chemical and physical stability, large exciton binding energy (60 meV), wide band gap, intensive ultraviolet (UV) and infrared (IR) adsorption [2–5]. ZnO NPs also have several advantages due to low toxicity, biosafe biocompatibility and biodegradability, which make the material important for antibacterial, antifungal, and wound healing applications [6–9].

Several studies have been conducted on various factors affecting

the shape, size, optical properties and applications of ZnO NPs. The factors are precursor concentrations [10], temperature [11, 12], surfactant concentrations [13, 14], dopant concentrations [15], solvent medium and pH of the reaction mixture [16, 17]. Doping is one of the strategies to modify the structural, morphological and optical properties of ZnO nanoparticles and enhance its applications such as antimicrobial activity.

In addition, several available reports deal with the particle size-dependent antimicrobial activity of ZnO nanoparticles (NPs), where antimicrobial activity is inversely related to the particle size. Hence, the crystal size of ZnO nanoparticles needs to be reduced for better antimicrobial activity [18]. The antimicrobial activity of undoped and doped zinc oxide nanoparticles has also been studied against gram-negative and gram-positive bacteria using chemically synthesizing method [19]. The main mechanism of antimicrobial activities of ZnO NPs is the electrostatic interaction between ZnO NPs and cell membrane of the bacteria, penetration of ZnO NPs into the inside of bacterial cell wall, and the formation of reactive oxygen species (ROS) inside the cell of bacteria, which destroys the cytoplasm of the bacteria [20]. It is reported that gram-negative bacteria are more resistant against ZnO NPs than gram-positive bacteria due to that it has double cell membrane structure (outside and cytoplasmic membrane) and the difference in intracellular antioxidant content [21].

Many researchers reported the synthesis and characterization of zinc oxide nanoparticle doped metals in separate studies for different precursors at different conditions using different synthesis methods. But, to date results there is a controversy and debate on the influence of these dopants on the structural, morphological and optical properties as well as on the antimicrobial activity of ZnO nanoparticles. Therefore, in this research, it is intended to investigate the effects of Mn and Gd dopant ions on the structural, morphological and optical properties of ZnO nanoparticle and on its antimicrobial activity.

2. MATERIALS AND METHODS

2.1. Materials

The precursor chemicals for the synthesis of pure and doped ZnO NPs are zinc acetate dihydrate (Unichem, India), sodium hydroxide (Alpha Chemika, India), Manganese acetate dihydrate (Unimag. media, India) and Gadolinium chloride hexahydrate (uni. Himedia, India). Culture media such as Müller–Hinton agar (M173-500G HiMedia, India), tryptone soya agar (T131-500G HiMedia, India), and nu-

trient broth (N173-500G HiMedia, India) for cultivation of the test organisms and used for the determination of antimicrobial activity of ZnO nanoparticles. Dimethyl sulfoxide (Unichem, India), ethanol and double distilled water were used as the solvent. Antibiotic gentamicin was used as positive control. All chemicals are analytical grades and do not undergo further purification.

2.2. Synthesis Methods

For synthesis of pure ZnO, 21.95 g of zinc acetate dihydrate was completely dissolved in 100 ml of deionized water and 0.2 M of aqueous NaOH solution was added drop wise to the mixture. Later, the solution was stirred for 30 minutes and placed at room temperature for 5 hrs for precipitation to occur. This one resulted in the formation of white coloured precipitates in the reaction mixture. In order to separate the precipitates, the reaction mixture was filtered and washed several times using double distilled water and ethanol to remove impurities. Finally, it was oven-dried at 60°C for 17 hrs. The calcination of the white powder was performed at 200°C for 2 hrs in a muffle furnace (model No. MC2-5/5/10-12, Biobase, Chine).

Similarly, to prepare Mn and Gd ion doped ZnO NPs we followed the already developed procedures by [22]. In order to synthesis of $Zn_{0.98}Mn_{0.02}O$ nanoparticle, 0.54 g of manganese acetate dehydrate was dissolved in 100 ml of deionized water and it was mixed with an aqueous zinc acetate dihydrate solution (21.95 g of zinc acetate dissolved in 100 ml of deionized water). 0.2 M of NaOH solution was added drop by drop to the above homogenous mixture to get a white precipitate with pale green colour. For drying and calcination, similar procedures mentioned above were repeated. Similarly, for the synthesis of $Zn_{0.98}Gd_{0.02}O$ nanoparticle, 0.5478 g of gadolinium chloride hexahydrate was dissolved in ethanol: double distilled water (50%:50%) and it was mixed with zinc acetate dihydrate solution (21.95 g of zinc acetate in 100 ml of deionized water).

2.3. Characterizations

X-ray diffractometer (XRD-7000, Shimadzu Co., Japan) to investigate the x-ray diffraction pattern of NPs by generating CuK_α radiation, $\lambda = 1.54056$ operating at a voltage of 40 kV and applied current of 30 mA. It is used to determine the crystalline phase of the undoped, Mn and Gd-doped ZnO nanoparticles. Intensities were measured at room temperature at an angle range of $2\theta = 10° \leq 2\theta \leq 80°$. All the diffraction peaks are well indexed to the

hexagonal ZnO wurtzite structure (JCPDS 36-1451). The average crystallite size estimated from the Debye–Scherrer formula [23]:

$$D = \frac{k\lambda}{\beta \cos\theta}, \tag{1}$$

where λ, θ, β and D are x-ray wavelength, Bragg's diffraction angle, full width at half maximum of the peak and average grain size of the crystallite, respectively. The lattice parameters a and c and the spacing distance d_{hkl} for the wurtzite structure of ZnO were calculated using Eqs. (2) and (3):

$$a = \frac{1}{\sqrt{3}} \frac{\lambda}{\sin\theta}, \tag{2}$$

$$c = \frac{\lambda}{\sin\theta}. \tag{3}$$

The dislocation densities (δ), the micro-strain (ε), the volume (V) of the unit cell for hexagonal system, the bond lengths (L), and the positional parameter (u) of undoped and doped ZnO nanoparticles were calculated by using Eqs. (4)–(8) [24]:

$$\delta = \frac{1}{D^2}, \tag{4}$$

$$e = \frac{\beta \cos\theta}{4}, \tag{5}$$

$$V = 0.88a^2c, \tag{6}$$

$$L = \sqrt{\left(\frac{a^2}{3} + \left(\frac{1}{2} - u\right)^2 c^2\right)}, \tag{7}$$

$$u = \frac{a^2}{3c^2} + 0.25. \tag{8}$$

The morphology of undoped and doped ZnO NPs was studied using a scanning electron microscope (Hitachi, H 7600). In SEM characterization, powder was mounted on a sample holder coating with a conductive metal. The samples were scanned with focused fine beams of electrons. The surface characteristics of the sample were obtained from the secondary electrons emitted from the sample surface [25].

The optical characterization of ZnO NPs was carried out using UV-Vis spectroscopy. The band gap energies are calculated using Eq. (9) [26]:

$$E_g = \frac{hc}{\lambda} = \frac{1240}{\lambda_{\max}} eV\,, \tag{9}$$

where h is the Planck's constant ($6.626 \cdot 10^{-34}$ J·s), c is the light velocity ($3 \cdot 10^8$ m/s), and λ is the wavelength.

2.4. Determination of Antimicrobial Activity of ZnO NPs

The antimicrobial properties of undoped, Mn-doped and Gd-doped ZnO nanoparticles were determined against gram-negative bacteria (*E. coli and P. aeruginosa*), gram-positive bacteria (*S. aureus and B. subtilis*) and fungus (*C. albicans*) using agar-well diffusion method. Dimethyl sulfoxide and standard antibiotic gentamicin were used as negative and positive control for the bacterial strains respectively. The strains were transferred to nutrient broth and incubated to grow aerobically at 37°C for 24 h until it achieved the turbidity of 0.5 McFarland standards. 0.01 mL of each sub-cultured bacteria were spread using sterilized cotton swab on 20 mL of sterilized molten and cooled MHA and TSA media, respectively. Subsequently, agar wells of 5 mm diameter were prepared on different plates with sterilized stainless steel cork borer and labelled properly. Different concentrations of (100, 150 and 200 μg/ml) of solutions were added into well using micropipette. The plates containing the microbes and nanoparticles were incubated at 37°C for 24 hrs in case of bacteria and 28°C for 48 hrs in case of yeast. The plates were examined for evidence of zones of inhibition, which appear as a clear area around the wells. The diameter of zones' inhibition measured and means value expressed in millimetres and compared with the standard drug gentamicin. All experiments were performed three times and the results were averaged.

3. RESULTS AND DISCUSSION

3.1. X-Ray Diffraction (XRD) Analysis

The structural analyses of pure ZnO and doped ($Zn_{0.98}Mn_{0.02}O$ and $Zn_{0.98}Gd_{0.02}O$) nanoparticles are depicted in Fig. 1, *a*–*c*. The diffraction peaks observed at $2\theta = 31.7480°$, 34.4191°, 36.2366°, 36.6165°, 47.5244°, 56.5660°, 56.8454°, 62.8533°, 66.3569°, 67.9250°, 69.0605° and 76.9425° correspond to (100), (002), (101), (102), (110), (103), (200), (112), (201), (004) and (202) planes, respectively. All the diffraction peaks are attributed to wurtzite structure of ZnO as compared to JCPDS file for ZnO (JCPDS card No. 36-1451) with space group $P63mc$ and lattice parameters $a = b = 3.25$ Å and

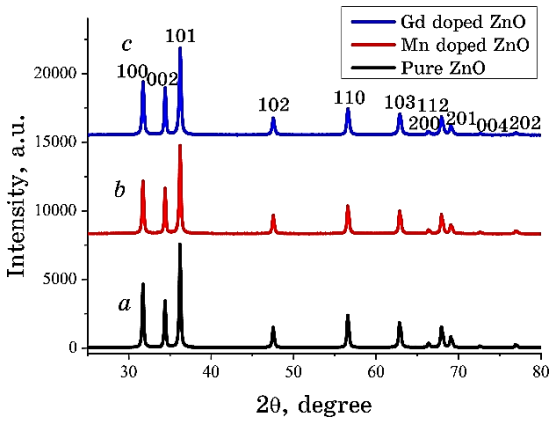

Fig. 1. X-ray diffraction patterns of (*a*) pure ZnO, (*b*) $Zn_{0.98}Mn_{0.02}O$- and (*c*) $Zn_{0.98}Gd_{0.02}O$-doped NPs.

$c = 5.206$ Å, which is in good agreement with previous reported in the literature [27, 28]. The sharp peaks and high diffracted intensity clearly indicated the crystalline nature of the particles. Similar patterns were also observed for Mn and Gd-doped ZnO NPs. The XRD results have no peaks correspond to Mn and Gd as well as MnO and Gd_2O_3 confirmed that Mn^{+2} and Gd^{+3} ions have clearly replaced the Zn^{2+} without introducing any impurities into the ZnO host lattice. On the other hand, the incorporation of Mn and Gd ions into ZnO host lattice or the replacement of Zn ions by Mn and Gd ions results in decrease the intensity of (101) peak which depicts that the decrease in the degree of crystallinity of samples as concentration of the defects in the sample increases [29].

The peak shift of (100), (002) and (101) are analysed using XRD. It is clearly seen that the FWHM slightly increases after adding the Mn and Gd dopants, indicating the growth of constrain of the crystalline or changes in the crystal strains according to the theory stated Eq. (5). In addition, peaks of (100), (002) and (101) slightly shift towards higher angles compared to undoped. The peak (100) is shifted from 31.7480° to 31.7506°, 31.7604° for $Zn_{0.98}Mn_{0.02}O$ and $Zn_{0.98}Gd_{0.02}O$, respectively. Similarly, the peak of (002) is shifted from 34.4191° to 34.4304°, 34.4359° for $Zn_{0.98}Mn_{0.02}O$ and $Zn_{0.98}Gd_{0.02}$, respectively. In the case of (101), it is shifted from 36.2366° to 36.2419° and 36.2532° for $Zn_{0.98}Mn_{0.02}O$ and $Zn_{0.98}Gd_{0.02}O$, respectively. Such a shifting of the XRD peaks depicts a lattice contraction and is attributed to the strain of the compound and mismatch of the ionic radii of Gd^{3+} (1.95°), Mn^{2+} (0.66°) and Zn^{2+} (0.74°) or replacement of some Zn cations with Mn and Gd ions in each compound [30].

On the other hand, the shift in the diffraction peaks is ascribed to the decrease in the crystallite size after the doping of Gd and Mn into the ZnO host lattice which results in the replacement of Zn ion with Gd and Mn ions and the formation of compression stresses in the ZnO that cause the positive shift of the ZnO peak. The positive shift indicates that when Gd and Mn are introduced into the ZnO matrix, the lattice contracts and the lattice parameter decreases. Thus, the positive peak shift is an indicator of incorporation of Mn and Gd dopants into the Zn sites [31].

The average crystallite size was estimated using Debye–Scherrer formula (1) and found to be 38, 36 and 31 nm for pure ZnO and Mn-, Gd-doped ZnO, respectively. The average crystallite size of Mn- and Gd-doped ZnO NPs is smaller as compared to pure ZnO NPs. FWHM of diffraction peak of ZnO (101) increases for Mn and Gd dopants; consequently, the size of nanoparticles decreases which is in agreement with results reported in literature [32]. The decrease in the crystallite size is attributed to the decrease in nucleation and growth of ZnO nanoparticles with the doping.

The values of lattice parameters (a, c), unit cell volume, bond length and positional parameter are calculated using Eqs. (2)–(8) shown in Table 1. It is observed that the unit cell volume, lattice parameters and the bond length slightly decreased after Mn and Gd doping, which might result from the difference in the ionic radii of Zn^{2+}, Mn^{2+} and Gd^{3+}, respectively. The smaller ionic radius of Mn^{2+} than Zn^{2+} results in the decrement of lattice parameter values of a and c whereas for larger ionic radius of Gd^{3+} than Zn^{2+} the increment of lattice parameter values of a and c would be expected but decreased due to strain as shown in Table 2. This slight variation in the lattice parameters of $Zn_{0.98}Mn_{0.02}O$ and $Zn_{0.98}Gd_{0.02}O$ is due to the substitution of Gd and Mn ions with different ionic radii. The slight variation in the aspect ratio (c/a) suggests that the Mn and Gd dopant ions are well substituted into the ZnO crystal lattice and indicated that the hexagonal wurtzite structure of ZnO is not altered due to Mn and Gd dopant ions [31]. The volume of the unit cell of doped ZnO NPs is decreased due to decrement of the lattice parameters after doping. The calculated values are 47.61, 47.50 and 47.01 $Å^3$ for ZnO, $Zn_{0.98}Mn_{0.02}O$ and $Zn_{0.980}Gd_{0.02}O$ respectively. This indicates that the addition of dopant ions into host lattice occupy partially in tetrahedral Zn positions. There is a strong correlation between c/a ratio and u. In this study, the c/a ratio reveals small perturbation for Mn and Gd doped ZnO NPs. The values of c/a and u parameters are given in Table 2. Moreover, the substitution of Mn and Gd ions results in significant changes in Zn–O bond length. From the Table 1, it is observed that the Zn–O bond length of pure ZnO NP is 1.979 Å. The bond length values decreased with Mn and

TABLE 1. Lattice parameters, cell volume and bond length of pure ZnO, $Zn_{0.98}Mn_{0.02}O$ and $Zn_{0.980}Gd_{0.02}O$ nanoparticles.

No.	Samples	Lattice parameters		Volume (V), Å^3	Positional parameters (u)	Zn–O-bond length (L), Å
		a, Å	c, Å			
1	undoped ZnO	3.250	5.206	1.601	0.379	1.979
2	Mn/ZnO	3.240	5.204	1.606	0.379	1.973
3	Gd/ZnO	3.230	5.202	1.600	0.379	1.968

TABLE 2. Dislocation densities and microstrain of undoped ZnO, $Zn_{0.98}Mn_{0.02}O$ and $Zn_{0.98}Gd_{0.02}O$ nanoparticles.

Samples	Dislocation density, lines/m^2	Microstrain, $\times10^{-4}$
pure ZnO	$6.9252{\cdot}10^{+14}$	7.72
$Zn_{0.98}Mn_{0.02}O$	$7.7160{\cdot}10^{+14}$	7.98
$Zn_{0.98}Gd_{0.02}O$	$1.0405{\cdot}10^{+15}$	9.37

Gd-doped ZnO samples due to the replacement of Zn^{2+} ions in ZnO lattice [33].

The reduction in the crystallite size is due to the distortion in a host ZnO lattice by the incorporation of foreign impurities and the presence of Mn^{2+} and Gd^{3+} into host lattice sites hinders the nucleation and subsequent growth rate of ZnO NPs. The substitution of Mn^{2+} and Gd^{3+} ions in the interstitial positions of host ZnO lattice influences the concentration of the interstitial Zn, O and Zn vacancies. The detection of small changes in 2θ values and peak broadening of diffraction peaks are due to the increase of microstrain and line broadening effect caused by size and microstrain of NPs.

The dislocation densities and microstrain of ZnO NPs were calculated from Eqs. (4), (5) [33], and given in Table 2. Comparably, the microstrain values increase for Mn^{2+} and Gd^{3+} doped ZnO NPs due to the relaxation of strain in the respective unit cells, which alters the size and shape of the particles [34].

3.2. Scanning Electron Microscopy (SEM) Analysis

The morphologies of undoped, Mn- and Gd-doped ZnO nanoparticles were studied using SEM images. Figures 2, *a*–*c* show the morphologies of ZnO, $Zn_{0.98}Mn_{0.02}O$ and $Zn_{0.98}Gd_{0.02}O$ NPs respectively. The particle agglomeration as well as narrow particle size distribution is observed in all of the samples. Scanning Electron Microscopy (SEM) images showed spherical shape with well-defined distributions were

observed [34].

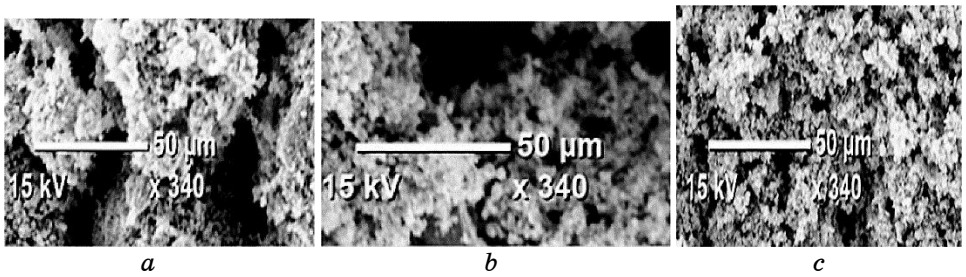

Fig. 2. SEM images of (*a*) undoped ZnO, (*b*) $Zn_{0.98}Mn_{0.02}O$ NPs, and (*c*) $Zn_{0.98}Gd_{0.02}O$ NPs. The particle agglomeration as well as narrow particle size distribution is observed in all of the samples.

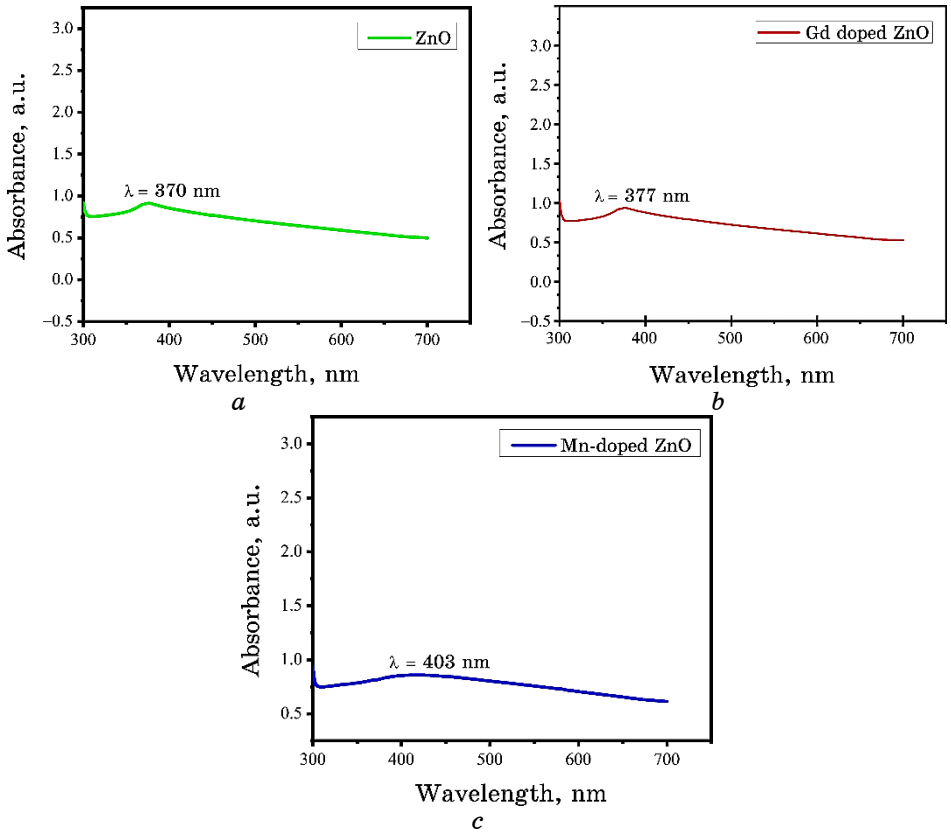

Fig. 3. The ultraviolet-visible absorption spectra of (*a*) pure ZnO, (*b*) $Zn_{0.98}Gd_{0.02}O$ NPs, and (*c*) $Zn_{0.98}Mn_{0.02}O$ NPs.

3.2. UV-Vis Spectroscopy Analysis

The effect of Mn and Gd doping on the optical properties NPs are shown in Fig. 3, *a*–*c*. The absorption peaks are observed at the wavelength of 370, 377 and 403 nm for undoped ZnO, $Zn_{0.98}Gd_{0.02}O$ and $Zn_{0.98}Mn_{0.02}O$, respectively. The corresponding optical band gap energy calculated using Eq. (9) was found to be 3.35, 3.28 and 3.07 eV, respectively. The ultraviolet absorption peaks regions are due to transition of electrons from valence band (VB) to conduction band (CB) [35]. It is observed that ZnO NP exhibited blue shifted absorbance peak as compared to its bulk counterpart having absorbance peak at 386 nm (3.2 eV) at room temperature. On another hand, decrease in the energy band gap of ZnO NPs with the doping of Mn and Gd ions, and this shift is ascribed to the influence of dopant ions. The interaction of d electron of Mn ion and f electron of Gd ion with *sp*-electron of ZnO may cause the dopant-induced states within the energy gap of ZnO NPs. These states correspond to the dopant additional pathways for electronic transition, thus, giving rise to the red shift of absorption due to incorporation of Mn^{2+} and Gd^{3+} ions into ZnO matrix [36].

3.3. Antimicrobial Studies

Figures 4, *a*–*e* demonstrate antimicrobial activity of pure ZnO, $Zn_{0.98}Mn_{0.02}O$ and $Zn_{0.98}Gd_{0.02}O$ nanoparticles against different pathogens (*P. aeruginosa*, *E. coli*, *S. aureus*, *B. subtilis*, and *C. albicans*) at the concentrations of 100, 150 and 200 μg/ml. The mechanism of antimicrobial activity are attributed to the release of Zn^{2+}, Mn^{2+} and Gd^{3+} ions in dissolution as well as the electrostatic attraction between negatively charged bacterial cells and positively charged nanoparticles, internalization into the bacterial cell wall and formation the reactive oxygen species (ROS) such as H_2O_2, hydroxyl radical OH^-, superoxide anion radical O_2^-, which cause damage to intracellular components such as DNA and cellular proteins, and may even lead to cell death [18–20]. The effects of concentrations on the antimicrobial activity of ZnO NPs are illustrated in Tables 3–5. It is observed that the zone of inhibition increases as the concentrations of NPs increases for both pure and doped NPs.

The interaction between the NPs and the cell wall of bacteria has been changed due to doping of Mn and Gd. Doping Mn and Gd with ZnO may lead to the variation in grain size, optical, morphology, and solubility of Zn^{2+} ions. All these factors have a significant effect on the antibacterial activity of ZnO [18–20]. In this study, the antimicrobial activity of ZnO NPs is increased with decreasing size of the crystal and energy band gap. It is observed that $Zn_{0.98}Gd_{0.02}O$

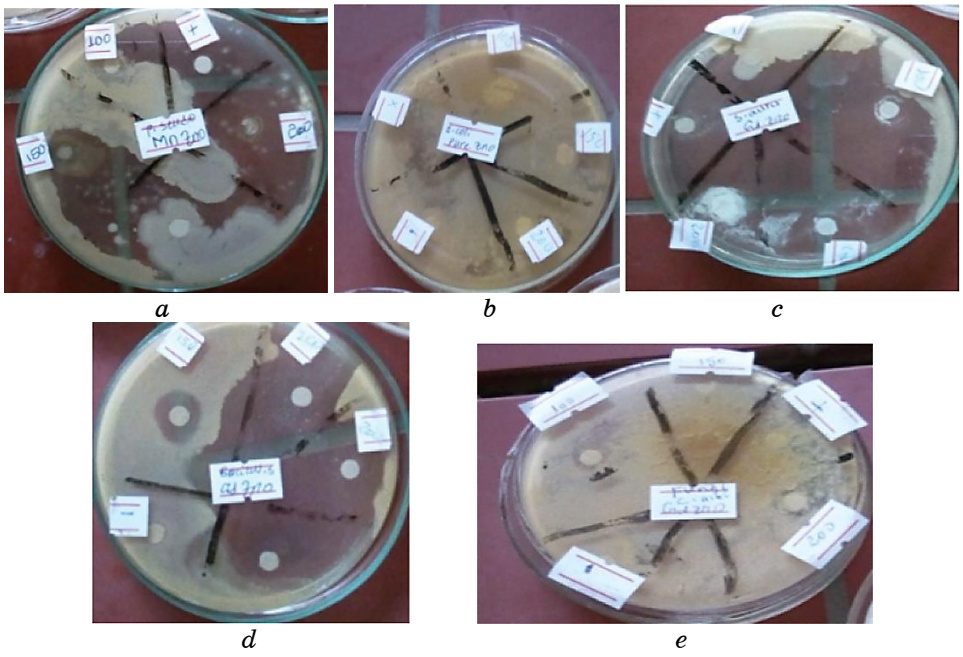

Fig. 4. The antimicrobial activities of (*a*) $Zn_{0.98}Mn_{0.02}O$ NPs applied on *P. aeruginosa*, (*b*) pure ZnO NPs applied on *E. coli*, (*c*) $Zn_{0.98}Gd_{0.02}O$ NPs applied on *S. aureus*, (*d*) $Zn_{0.98}Gd_{0.02}O$ NPs applied on *B. subtilis*, and (*e*) $Zn_{0.98}Gd_{0.02}O$ NPs applied on *C. albicans* with different concentrations (100, 150 and 200 μg/mL).

showed better antimicrobial activity than $Zn_{0.98}Mn_{0.02}O$ and undoped ZnO due to its small size as shown in Tables 3–5. A large number of studies investigated on the considerable impact of particle size on the antibacterial activity, and the researchers found that controlling ZnO-NPs' size was crucial to achieve best bactericidal response, and ZnO NPs with smaller size (higher specific surface areas) showed highest antibacterial activity [20].

The growth of all bacteria and fungus are more affected by Gd^{3+}- and Mn^{2+}-doped ZnO nanostructures as compared with pure ZnO NPs. The other reason for the increment of antimicrobial activity of Gd doped ZnO NPs is ascribed to large generation of ROS species as doping creates a large number of defects which increases ROS species and consequently it increases antimicrobial activity. In general, nanoparticles with better photocatalytic activity have larger specific surface areas and smaller crystallite sizes, which increase oxygen vacancies, resulting in more ROS. Furthermore, due to the various surface–interface characteristics may have different chemical–physical, adsorption–desorption abilities in the direction towards

TABLE 3. Zones of inhibition of ZnO, $Zn_{0.98}Mn_{0.02}O$ and $Zn_{0.98}Gd_{0.02}O$ on different types of pathogens with concentration of 100 μg/mL.

Types of pathogens	Zones of inhibition [mm] at the concentration of 100 μg/ml of NPs			
	undoped ZnO	$Zn_{0.98}Mn_{0.02}O$	$Zn_{0.98}Gd_{0.02}O$	gentamicin (+control)
E. coli	5	8	18	19
P. aeruginosa	6	5	15	17
B. subtilis	7	10	20	28
S. aureus	7	15	19	29
C. albicans	4	10	15	21

TABLE 4. Zones of inhibition of ZnO, $Zn_{0.98}Mn_{0.02}O$ and $Zn_{0.98}Gd_{0.02}O$ on different types of pathogens with concentration 150 μg/mL.

Types of pathogens	Zones of inhibition [mm] at the concentration of 150 μg/mL of NPs			
	undoped ZnO	$Zn_{0.98}Mn_{0.02}O$	$Zn_{0.98}Gd_{0.02}O$	gentamicin (+control)
E. coli	8	10	20	19
P. aeruginosa	7	10	15	17
B. subtilis	8	17	25	28
S. aureus	9	20	25	29
C. albicans	6	10	20	21

bacteria, make sure in different antibacterial performances. The results have revealed that Gd- and Mn-doped ZnO nanostructures will be a promising candidate to be used for potential drug delivery systems to cure some significant infections [37, 38].

In the present study, we also found that gram-positive bacteria were more sensitive than gram-negative bacterial strains and fungus against the NPs tested as shown in Tables 3–5 for different concentrations. All NPs that means pure ZnO, Mn- and Gd-doped ZnO NPs were more sensitive to *S. aureus* and *E. coli* as indicated in tables. The more activity of NPs towards gram-positive bacteria is ascribed to the difference in their structure and chemical composition. The cell wall of gram-positive bacteria has single membrane whereas the gram-negative bacteria cell wall has outside and inside cytoplasmic membrane as well as lipopolysaccharide, which covers peptidoglycan. Therefore, in this case gram-positive bacteria cell surface results in more destruction and cell death than gram-negative bacteria. It was also reported earlier that various bacterial strains had considerably different infectivity and tolerance levels

TABLE 5. Zones of inhibition of ZnO, $Zn_{0.98}Mn_{0.02}O$ and $Zn_{0.98}Gd_{0.02}O$ on different types of pathogens with concentration 200 μg/mL.

Types of pathogens	Zones of inhibition [mm] at the concentration of 200 μg/mL of NPs			
	undoped ZnO	$Zn_{0.98}Mn_{0.02}O$	$Zn_{0.98}Gd_{0.02}O$	gentamicin (+control)
E. coli	9	10	20	19
P. aeruginosa	8	10	15	17
B. subtilis	10	18	30	28
S. aureus	11	22	29	29
C. albicans	6	18	21	21

towards the different agents including antibiotics [39].

4. CONCLUSIONS

The structural, morphological and optical properties of ZnO nanoparticle doped with manganese (Mn) and gadolinium (Gd) ions, and their antimicrobial activity were investigated.

The nanoparticles were characterized by XRD, SEM and UV-vis spectroscopy. The XRD result revealed that the synthesized ZnO NPs were in nanometre range with average crystallite size of about 31–38 nm from the Scherrer's formula. The lattice parameters, unit cell volume and bond lengths were decreased with the doping with Gd and Mn. On the other hand, physical defects and dislocations were increased. It was also perceived that XRD peaks shifted to higher diffraction angles due to the difference of the ionic radii of Mn^{2+}, Zn^{2+} and Gd^{3+}. Morphological studies obtained from SEM have revealed the formation of spherical nanoparticles for all samples. Optical band gap energy was found to be decreased with doping due to the introduction of new energy levels in the energy band gap.

The zone of inhibition was observed against pathogenic bacteria and fungus strains and suggests that $Zn_{0.98}Gd_{0.02}O$ and $Zn_{0.98}Mn_{0.02}O$ showed good antimicrobial activity on gram-positive bacteria (*S. aureus* and *B. subtilis*), gram-negative bacteria (*E. coli* and *P. aeruginosa*) and fungus (*C. albicans*) than the undoped ZnO nanoparticles.

In addition, the results of this study depicted that the antimicrobial activities of synthesized NPs were increased with the concentration and size decrement of the crystal. Furthermore, the results indicated that the gram-positive bacteria were more sensitive to all undoped, Mn- and Gd-doped ZnO NPs than gram-negative bacteria and fungus.

ACKNOWLEDGMENTS

The authors would like to acknowledge Adama Science and Technology University and the Ministry of Innovation and Technology of Ethiopia for financial support. We also like to appreciate the Biology Department of Adama Science and Technology University for allowing us to use UV-Vis spectroscopy and SEM facilities.

REFERENCES

1. M. Kasahun, A. Yadate, A. Belay, Z. Belay, and M. Ramalingam, *Nano Biomed. Eng.*, **12**, No. 1: 47 (2020); doi:10.5101/nbe.v12i1.p47-56
2. S. K. Mihra, R. K. Srivastava, and S. G. Prakash, *Journal of Alloys and Compounds*, **539**: 1 (2012); doi:10.1016/j.jallcom.2012.06.024
3. J. Wang, J. Cao, B. Fang et al., *Mater Lett.*, **59**: 1405 (2005); https://doi.org/10.1016/j.matlet.2004.11.062
4. Z. L. Wang, *ACS Nano*, **2**: 1987 (2008); https://doi.org/10.1021/nn800631r
5. M. Chaari and A. Matoussi, *Phys. B: Condensed Matter*, **407**: 3441 (2012); doi:10.1016/j.physb.2012.04.05
6. J. Ma, J. Liu, Y. Bao et al., *Ceram. Int.*, **39**, No. 3: 2803 (2013); https://doi.org/10.1016/j.ceramint.2012.09.049
7. P. Jamdagni, P. Khatri, and I. S. Rana, *Journal of King Saud University Science*, **2018**: 168 (2018); https://doi.org/10.1016/j.jksus.2016.10.002
8. R. Jalal, M. Abareshi, E. K. Goharshadi et al., *Materials Chemistry and Physics*, **121**, Nos. 1–2: 198 (2010); doi:10.1016/j.matchemphys.2010.01.020
9. J. Podporska-Carroll, A. Myles, B. Quilty et al., *J. Hazard Mater.*, **324**: 39 (2017); doi.org/10.1016/j.jhazmat.2015.12.038
10. P. Chand, A. Gaur, A. Kumar et al., *Appl. Surf. Sci.*, **356**: 438 (2015); https://doi.org/10.1016/j.apsusc.2015.08.107
11. M. Jyoti, D. Vijay, and S. Radha, *IJSRP*, **3**: 1 (2013).
12. G. N. Narayanan, R. S. Ganesh, and A. Karthigeyan, *Thin Solid Films*, **598**: 39 (2016); https://doi.org/10.1016/j.tsf.2015.11.071
13. Y. L. Zhang, Y. Yang, J. H. Zhao et al., *J. Sol–Gel Sci. Technol.*, **51**: 198 (2009); https://doi.org/10.1007/s10971-009-1959-5
14. A. Bera and D. Basak, *ACS Appl. Mat. Interfaces*, **1**: 2066 (2009); https://doi.org/10.1021/am900422y
15. A. Naskar, S. Lee, and K. Kim, *RSC Adv.*, **10**: 1232 (2020); doi:10.1039/C9RA09512H
16. A. Bagabas, A. Alshammari, M. F. A. Aboud et al., *Nanoscale Res. Lett.*, **8**: 516 (2013); https://doi.org/10.1186/1556-276X-8-516
17. R. Wahab, S. G. Ansari, Y. S. Kim et al., *Appl. Surf. Sci.*, **255**: 4891 (2009); https://doi.org/10.1016/j.solmat.2008.06.019
18. A. Sirelkhatim et al., *Nanomicro Lett.*, **7**, No. 3: 219 (2015); https://doi.org/10.1007/s40820-015-0040-x
19. A. J. Ahmed, *Int. Res. J. Pharm.*, **9**, No. 9: 16 (2018), doi:10.7897/2230-8407.099181
20. P. Narayanan, W. S. Wilson, A. T. Abraham, and M. Sevanan, *BioNanoSci-*

ence, **2**, No. 4: 329 (2012); doi:10.1007/s12668-012-0061-6
21. S. Getie, A. Belay, A. R. Chandra Reddy, and Z. Belay, *Journal of Nanomedicine & Nanotechnology*, **S8**: 1 (2017); doi:10.4172/2157-7439.S8-004
22. Sh. Jeetendra, H. Nagabhushana, K. Mrudula, C. S. Naveen, P. Raghu, and H. M. Mahesh, *Int. J. Electrochem. Sci.*, **9**: 2944 (2014).
23. R. Jenkins and R. L. Synyder, *Introduction to X-Ray Power Diffractometry* (New York: John Wiley and Sons: 1996)
24. O. Bilgili, *Acta Physica Polonica A*, **136**: 79 (2019); doi:10.1109/SMELEC.2010.5549430
25. W. Zhou, R. Apkarian, Z. L. Wang, and D. Joy, *Fundamentals of Scanning Electron Microscopy (SEM), Scanning Microscopy for Nanotechnology: Techniques and Applications* (New York: Springer: 2007), p. 1.
26. A. Khorsand Zak, M. Ebrahimizadeh Abrishami, W. H. Abd. Majid, Ramin Yousefi, S. M. Hosseini, *Ceramic International*, **37**: 393 (2011); https://doi.org/10.1016/j.ceramint.2010.08.017
27. A. B. Gemta, B. Bekele, and A. R. C. Reddy, *Digest Journal of Nanomaterials and Biostructure*, **214**: 51 (2019).
28. P. Ghosh and A. K. Sharma, *Journal of Nanomaterials*, **2013**: ID 480164 (2013); https://doi.org/10.1155/2013/480164
29. Y. Abdollahi, A. H. Abdullah, Z. Zainal, and N. A. Yusof, *International Journal of Basic & Applied Sciences IJBAS-IJENS*, **11**, No. 4: 62 (2015).
30. R. K. Sharma, S. Patel, and K. C. Pargaien, *Adv. Nat. Sci.: Nanosci. Nanotechnol.*, **3**: 035005 (2012); https://iopscience.iop.org/article/10.1088/2043-6262/3/3/035005
31. M. Sarfraz, N. Ahmed, K. U. Haq, S. H. SHahida, and M. A. Khana, *Materials Science-Poland*, **37**, No. 2: 280 (2019); https://doi.org/10.2478/msp-2019-0029
32. M. Aparecida, R. Bonifácio, H. d. L. Lira, L. S. Neiva, and L. Gama, *Materials Research*, **20**, No. 4: 1044 (2017); https://doi.org/10.1590/1980-5373-mr-2015-0765
33. G. Vijayaprasath, G. Ravi, A. S. Haja Hameed, and T. Mahalingam, *J. Phys. Chem. C*, **118**: 9715 (2014); https://doi.org/10.1021/jp411848t
34. S. D. Senol, B. Yalcin, E. Ozugurlu, and L. Arda, *Mater. Res. Express*, **7**: 015079 (2020).
35. J. H. Zheng, J. L. Song, Z. Zhao, Q. Jiang, and J. S. Lian, **47**, No. 7: 713 (2012); https://doi.org/10.1002/crat.201200026
36. S. S. Sartiman, N. F. Djaja, and R. Saleh, **4**: 528 (2013); doi:10.4236/msa.2013.49065
37. Sh. A. Khan, S. Shahid, W. Bashir, S. Kanwal, and A. Iqbal, *Tropical Journal of Pharmaceutical Research*, **16**, No. 10: 2331 (2017); http://dx.doi.org/10.4314/tjpr.v16i10.4
38. A. F. Fathima, R. J. Mani, K. Sakthipandi, K. Manimala, and A. Hossain, *Journal of Inorganic and Organometallic Polymers and Materials*, **30**, Iss. 7: 2397 (2019); https://doi.org/10.1007/s10904-019-01400-z
39. Z. E. Karvani and P. Chehrazi, *African Journal of Microbiology Research*, **5**, No. 2: 1368 (2011); doi:10.5897/AJMR10.159